



WRF-Hydro-CUFA: A scalable and adaptable coastal-urban flood model based on the WRF-Hydro and SWMM models

Youngjun Son^{a,*}, Emanuele Di Lorenzo^{a,b}, Jian Luo^c

^a Program in Ocean Science and Engineering, Georgia Institute of Technology, Atlanta, GA, USA

^b Department of Earth, Environmental, and Planetary Sciences, Brown University, Providence, RI, USA

^c School of Civil and Environmental Engineering, Georgia Institute of Technology, Atlanta, GA, USA

ARTICLE INFO

Handling Editor: Daniel P Ames

Keywords:

Urban flood
Coastal flood
Hyper-resolution
WRF-Hydro model
SWMM model
Operational flood predictions

ABSTRACT

An open-source urban flood model is vital for vulnerable coastal communities with limited budgets to assess emerging flood risks posed by global climate change. In this study, a hyper-resolution flood model for coastal-urban systems, WRF-Hydro-CUFA (Coastal Urban Flood Applications), is developed based on a distributed process-based hydrologic model, WRF-Hydro, to represent urban hydrologic processes. In addition, WRF-Hydro-CUFA integrates a hydraulic flow solver, SWMM, to consider flood controls of stormwater drainage. As a pilot study, the applications for past non-extreme and extreme flood events in the City of Tybee Island, USA, show that WRF-Hydro-CUFA can represent multiple flood mechanisms, including coastal and pluvial flooding. WRF-Hydro-CUFA is further implemented for operational flood predictions on a web-based dashboard, providing an opportunity for calibration and improvement. The application and enhancement processes of WRF-Hydro-CUFA can be transferred and adapted in other coastal communities facing similar flood risks but with limited access to flood models.

1. Introduction

Increasing flooding poses a greater threat to populations and communities in urban systems located in coastal floodplains (Hallegatte et al., 2013; Neumann et al., 2015). Flooding due to hurricane-induced storm surges led to a substantial loss of human lives, properties, and infrastructure (e.g., Rosenzweig and Solecki, 2014; Sebastian et al., 2017). In addition, as a consequence of global climate change, sea level rise and intensifying weather events increase the exposure of coastal communities to a risk of nuisance flooding (Sweet et al., 2017, 2022). Less extreme but frequent flooding in low-lying coastal areas chronically disrupts public services and local businesses by impeding traffic and damaging properties (Moftakhari et al., 2018). These impacts of flooding arise disproportionately in communities with demographic and socio-economic vulnerabilities during the preparation, response, and recovery phases (Masozera et al., 2007; Rufat et al., 2015; Buchanan et al., 2020). Inequitable access to flood-related resources and risk management exacerbates social and economic heterogeneity in adaptation to floods (Pelling and Garschagen, 2019; Moulds et al., 2021). While urban flood models play a key role in understanding flood dynamics and associated risks, most of the developments and applications

rely on short-term consulting projects exclusive to municipalities and private sectors (Rosenzweig et al., 2021). Consequently, there is a need for open-source urban flood models that are broadly available for coastal communities, as well as for further research and development.

In urban systems, floodwater accumulates on land when it exceeds the capacity of soil infiltration and stormwater drainage (National Academies, 2019). In many coastal areas, unsaturated soil layers become narrower with rising sea levels, which negatively affects the capability of soil columns to naturally drain excessive water on land (Bossierelle et al., 2022). In addition, rainfall or high tide events increase soil moisture and shallow groundwater levels and subsequently cause local areas more susceptible to flooding. Such preconditions for flooding can compound with other drivers of flooding to amplify the impacts, resulting in more extensive and lingering inundation (Santiago-Collazo et al., 2019; Zscheischler et al., 2020). Along coasts, sea level rise exposes an increasing number of stormwater outfalls to a risk of being partially or completely submerged (Habel et al., 2020). As a result, less extreme rainfall events can overwhelm stormwater drainage at high tailwater conditions, such as high tides, losing its engineered capability to quickly drain rainfall-runoff (Shen et al., 2019). Moreover, submerged stormwater outfalls allow saltwater to encroach into urban

* Corresponding author. 311 Ferst Drive, Atlanta, GA, 30332, USA.

E-mail address: youngjun.son@gatech.edu (Y. Son).

<https://doi.org/10.1016/j.envsoft.2023.105770>

Received 10 March 2023; Received in revised form 29 May 2023; Accepted 3 July 2023

Available online 4 July 2023

1364-8152/© 2023 Elsevier Ltd. All rights reserved.

systems and inundate the surrounding areas of stormwater inlets (National Academies, 2019; Habel et al., 2020). These flood pathways become progressively more important with changing climates and continuous urban development that alters land imperviousness and stormwater drainage networks. Therefore, the development of urban flood models needs to facilitate consistent monitoring and dedicated collaboration to support resilience strategies against emerging flood risks (Rosenzweig et al., 2021).

Urban flood models have been developed to represent the dynamics of overland floodwater flows resulting from various flood mechanisms and subsequent interactions in the built environment (see reviews in Salvatore et al., 2015; Teng et al., 2017; Gallien et al., 2018; Santiago-Collazo et al., 2019). Particularly for urban systems in coastal regions, a wide range of flood models have been applied at street-to-building scales to address different drivers of flooding, as summarized in Table 1. While urban flood models can take account of coastal or fluvial flood processes by linking with other dynamic models or gauge observations, accurate representations of pluvial and subsurface interactions are still challenging for many flood models to skillfully predict potential flooding in urban areas (Rosenzweig et al., 2021). For example, although subsurface layers of land provide an important buffer

in the accumulations of floodwater, an assumption of impervious land is common in many studies on coastal-urban flooding (e.g., Blumberg et al., 2015; Marsooli and Wang, 2020; Takagi et al., 2016; Gallien et al., 2014; Gallien, 2016; Shen et al., 2019; Smith et al., 2011; Yin et al., 2016). Only a few studies incorporated urban hydrologic processes, such as spatially-distributed precipitation and soil hydraulic properties, by using hydrologic models linked with coastal and fluvial flooding (e.g., Thompson et al., 2004; Joyce et al., 2017; Saksena et al., 2020; Karamouz et al., 2017; Silva-Araya et al., 2018). Karamouz et al. (2017) and Silva-Araya et al. (2018) implemented a distributed process-based hydrologic model, Gridded Surface/Subsurface Hydrologic Analysis (GSSHA) (Downer and Ogden, 2004), with floodwater sources along the coastlines based on the statistical estimations and regional-scale Advanced Circulation (ADCIRC) model simulations, respectively, to study the compounding effects of coastal water levels and precipitation.

In the built environment, floodwater has extensive feedback not only on urban hydrology but also on stormwater drainage (Ogden et al., 2011). For modeling stormwater drainage in flood simulations, a common approach is to couple a one-dimensional (1D) hydraulic model for drainage flows with a two-dimensional (2D) hydrodynamic model for overland flows (Rosenzweig et al., 2021). For example, based on the

Table 1

Summary of flood models for coastal-urban systems and comparison with WRF-Hydro-CUFA. The linked inputs were imposed along coastlines (C), upstream (U), downstream (D), or by precipitation (P).

Flood model (license)	Reference	Study location	Flood processes of interest	Linked inputs (boundary)	Urban hydrology	Stormwater drainage
sECOM (research)	Blumberg et al. (2015)	Hudson River Waterfront, NY, USA	Coastal (storm surge)	(C) 3-layer nested water levels	No infiltration	Not capable
ADCIRC & SWAN (open-source)	Marsooli and Wang (2020)	Manhattan, NY, USA	Coastal (storm surge)		No infiltration	Not capable
ADCIRC & SWMM (research)	Shi et al. (2022)	Xiangshan, China	Coastal, fluvial, pluvial	(P) gauge-based rainfall	Semi-distributed hydrology	Included
Delft3D (open-source)	Takagi et al. (2016)	Leyte Island, Philippines	Coastal (storm surge)		No infiltration	Not capable
BreZo (research)	Gallien et al. (2014)	Newport Beach, CA, USA	Coastal (wave overtopping)	(C) SWAN/empirical model	No infiltration	Empirical flow rates (only sinks)
	Gallien (2016)	Imperial Beach, CA, USA	Coastal (wave overtopping)	(C) SWAN & XBeach/empirical model	No infiltration	Not capable
TUFLOW (commercial)	Shen et al. (2019)	Norfolk, VA, USA	Coastal, pluvial	(C) & (P) statistical estimates	Uniform rainfall w/o infiltration	Included
LISFLOOD-FP (executables available)	Smith et al. (2011)	Somerset Coast, UK	Coastal	(C) tide gauges	No infiltration	Not capable
FloodMap* (research)	Yin et al. (2016)	Manhattan, NY, USA	Coastal	(C) ADCIRC	No infiltration	Not capable
HEC-RAS 2D (executables available)	Saleh et al. (2017)	Hackensack-Passaic Watershed, NY, USA	Fluvial, pluvial	(U) HEC-HMS, (D) sECOM, (P) GEFS ^a	Uniform rainfall excess	Not capable
UT-Arlington (research)	Noh et al. (2019)	Houston Metropolitan, TX, USA	Fluvial, pluvial	(D) tide gauge, (P) QPE ^b	Distributed rainfalls w/ runoff coefficients	Not included
MIKE SHE* & MIKE 11 (commercial)	Thompson et al. (2004)	The Isle of Sheppey, UK	Fluvial, pluvial, subsurface	(D) streamflow controls, (P) gauge-based rainfall	Distributed hydrology	Not included
ICPR (commercial)	Joyce et al. (2017)	Cross Bayou Watershed, FL, USA	Fluvial, pluvial, subsurface	(D) ADCIRC & SWAN, (P) statistical estimates	Distributed hydrology	Included by equivalent modeling
	Saksena et al. (2020)	Houston, TX, USA	Fluvial, pluvial	(U) streamflow gauges, (D) tide gauge, (P) NLDAS ^c	Distributed hydrology w/o subsurface flows	Not included
GSSHA* (executables available)	Karamouz et al. (2017)	Manhattan, NY, USA	Coastal, pluvial, subsurface	(C) & (P) statistical estimates	Distributed hydrology	Not included
	Silva-Araya et al. (2018)	Fajardo, PR, USA	Coastal, fluvial, pluvial, subsurface	(C) ADCIRC & SWAN, (P) radar-based rainfall	Distributed hydrology	Not included
WRF-Hydro-CUFA* (open-source)	Present study	Tybee Island, GA, USA	Coastal, pluvial, subsurface	(C) tide gauge, (P) QPE ^b	Distributed hydrology	Included

* Models with diffusive wave approximations for overland flows.

^a GEFS: Global Ensemble Forecast System.

^b QPE: Quantitative Precipitation Estimation.

^c NLDAS: North American Land Data Assimilation System.

open-source distributions, the Storm Water Management Model (SWMM) (Rossman, 2015) is widely adopted not only for research flood models but also for commercial packages for drainage design and planning (see a review in Niazi et al., 2017). The majority of coupled 1D-2D flood models have been developed for urban systems in inland regions where stormwater discharges are affected mostly during extreme river stages (e.g., the LISFLOOD-FP & SWMM model by Wu et al., 2017; the 2D SWM & SWMM model by Chen et al., 2018; the UT-Arlington model by Noh et al., 2018; the MIKE 21 & URBAN model by Hossain Anni et al., 2020). However, stormwater drainage networks in coastal communities are commonly found along low-gradient landscapes, with their outfalls located in the intertidal zones, thus encountering a frequent loss of drainage capability. Only a few studies applied coupled 1D-2D flood models to address the combined effects of coastal and pluvial flooding. Shen et al. (2019) used the TUFLOW model to map coastal and pluvial flood risks and their interactions with stormwater drainage for design storm scenarios. Shi et al. (2022) coupled the ADCIRC and SWMM models to identify the prominent flood risks in different areas and examine the effects of flood controls. Despite the growing demand for coupled 1D-2D flood models to understand and manage the impacts of climate change and urban development, only a limited number of open-source research flood models are available (Chen et al., 2018).

In this study, an open-source urban flood model, WRF-Hydro-CUFA (Coastal Urban Flood Applications), is developed to enable consistent flood risk management for vulnerable coastal communities in changing environments. With an emphasis on urban hydrology and stormwater drainage, the flood model is built based upon the Weather Research and Forecasting Hydrologic (WRF-Hydro) model (Gochis et al., 2020) for distributed process-based hydrologic predictions of coastal-urban flooding and coupled with the SWMM model to enable modeling of stormwater drainage. As implemented in the National Water Model (NWM) (NOAA NWS, 2016) for operational forecasts of streamflow in the United States, WRF-Hydro has the capability to efficiently represent multiple hydrologic processes of inland water cycles, including land-atmosphere interactions through the Noah/Noah-MP (Multi-Parameterization) Land Surface Model (LSM) (Niu et al., 2011; Yang et al., 2011) and runoff flow routings over lands, subsurface, and channels. Moreover, it is an open-source model with a significant advantage of scalability supporting the Message Passing Interface (MPI) parallelization for a High-Performance Computing (HPC) environment. By coupling between the WRF-Hydro and SWMM models, WRF-Hydro-CUFA can provide a better understanding of floodwater interactions with natural and engineered drainage systems for floods driven by high coastal water levels and precipitation. Table 1 also shows the comparison of WRF-Hydro-CUFA with other flood models for coastal-urban systems. As a pilot study of WRF-Hydro-CUFA, the City of Tybee Island in GA, USA, is selected due to its immediate flood risks with changing climates. Furthermore, a web-based dashboard for operational flood predictions is established based on WRF-Hydro-CUFA to narrow existing knowledge gaps associated with flood characteristics between the flood model development and local practices. As a framework, the development and operations of WRF-Hydro-CUFA will allow a coastal community to adapt and tailor its own flood model based on knowledge and experience of past and present flood events, which can be transferable to other vulnerable coastal communities with limited access to flood models. The framework will potentially contribute to understanding hydrologic responses of coastal-urban systems to floods and subsequently help identify emerging threats posed by climate change.

The remainder of the paper is outlined as follows. Section 2 describes the WRF-Hydro and SWMM models and additional modules in WRF-Hydro-CUFA to impose coastal water levels and to couple the WRF-Hydro and SWMM models. In addition, hyper-resolution modeling information is provided for a pilot study of the City of Tybee Island. In Section 3, we perform model simulations for stormwater inundation during perigean spring tides and for hurricane-induced compound

flooding, and compare the simulation results with available flood data. Section 4 demonstrates the model application to a web-based dashboard that provides flood predictions together with other flood-related resources. We discuss the model capability and opportunity for consistent management of emerging flood risks, as well as limitations, in Section 5. Finally, Section 6 concludes the study with a summary.

2. Methods

2.1. WRF-Hydro

WRF-Hydro (version 5.2.0) is a key basis of WRF-Hydro-CUFA that extends it to flood simulations in coastal-urban systems. As a distributed process-based hydrologic model, WRF-Hydro has an advantage in representing the spatially heterogeneous nature of hydrologic variables, such as meteorological forcing and land properties. WRF-Hydro consists of multiple routing modules for overland flow, saturated subsurface flow, baseflow, and streamflow to route surface and subsurface runoffs that are hydrologically partitioned from the integrated Noah/Noah-MP LSM. While WRF-Hydro has been primarily used to predict streamflow hydrograph in large watersheds, it has applications to study inland urban flooding in both high-resolution (>50 m) (e.g., 125 m by Kim et al., 2021) and hyper-resolution (<50 m) (e.g., 10 m by Smith et al., 2021), respectively. Since a detailed description of the WRF-Hydro modules can be found in Gochis et al. (2020), we describe only the primary hydrologic representations that are relevant to WRF-Hydro-CUFA.

Among the different surface-subsurface runoff schemes available in the Noah/Noah-MP LSM, the Simple Water Balance (SWB) model (Schaake et al., 1996) is selected in WRF-Hydro-CUFA as in the NWM. The SWB model determines infiltration excess based on the runoff equation of Moore (1985), or equivalently the Soil Conservation Service (SCS) curve number equation (Soil Conservation Service, 1972), with an exponential distribution for the infiltration capacity. Therefore, the runoff, Q_s , and infiltration capacity, I_c , are defined as Schaake et al. (1996):

$$Q_s = \frac{P_x^2}{(P_x + I_c)} \quad (1)$$

$$I_c = D_x(1 - e^{-kt}) \quad (2)$$

where P_x , D_x , and k denote the effective precipitation, soil moisture deficit, and decay coefficient for time, t , respectively. The infiltration capacity is analogous to the potential infiltration rate of the Horton infiltration model (Horton, 1941) without the equilibrium infiltration term (Kim et al., 2021). In Eq. (2), the decay coefficient is a key parameter to determine surface runoff (see Appendix A for the WRF-Hydro input). The infiltration capacity is also a function of the soil moisture deficit, D_x , which is determined by solving the Richards' equation with the Clapp-Hornberger relationship for soil water retention (Clapp and Hornberger, 1978). The hydrologic processes of the Noah/Noah-MP LSM are described in Niu et al. (2011) and Yang et al. (2011). For the lateral flows, the routing module for saturated subsurface flow solves the quasi-three-dimensional, Boussinesq equation with the steady-state approximation (Wigmosta et al., 1994; Wigmosta and Lettenmaier, 1999), based on the hydraulic gradients of shallow groundwater table depth. Supersaturated soil columns add exfiltration into infiltration excess on land prior to routing of overland flows. Then, the fully unsteady, spatially explicit, diffusive wave formulation (Julien et al., 1995; Ogden, 1997) is adopted along with the steepest-descent method to calculate overland flows for infiltration excess over maximum retention depths. The resulting surface water heads on land provide time-evolving flood depths and extents.

2.2. SWMM

SWMM is a rainfall-runoff simulation model that consists of semi-distributed hydrology, 1D hydraulics, and water-quality model components (Rossman, 2015). The 1D hydraulics model component uses a node-link representation to calculate water flows through a conveyance network of channels and pipes. The conservation of mass and momentum for unsteady free surface flows, namely the Saint-Venant equations, are solved for links based on a finite difference scheme:

$$\frac{\partial A}{\partial t} + \frac{\partial Q}{\partial x} = 0 \quad (3)$$

$$\frac{\partial Q}{\partial t} + \frac{\partial}{\partial x} \left(\frac{Q^2}{A} \right) + gA \frac{\partial h}{\partial x} + gA(S_f - S_0) = 0 \quad (4)$$

where Q is the flow rate, A is the cross-sectional flow area, h is the flow depth, S_f is the friction slope, and S_0 is the pipe slope. Then, the conservation of mass is applied for a node assembly – one node and half-links connected to it. Each time a new flow rate is calculated, flow limiting conditions are checked based on the slope, upstream, and downstream limiting criteria. For example, if a backflow preventer (e.g., a flap gate) is assigned to a link, the net flow is set to zero when the calculated flow rate is negative (flowing upstream). SWMM integrates a set of empirical equations and properties for hydraulic elements, such as pumps, orifices, and weirs. The details of numerical methods and handling options for hydraulic parameters can be found in Rossman (2015).

2.3. Model development of WRF-Hydro-CUFA

As outlined in the flowchart in Fig. 1, WRF-Hydro-CUFA uses only the Noah-MP LSM and terrain-routing modules for overland and saturated subsurface flows of WRF-Hydro. For its application for coastal-urban flood simulations, WRF-Hydro-CUFA has two additional implementations, one module to introduce spatially- and temporally-varying water levels as coastal boundary conditions and the other to pair floodwater information with SWMM for stormwater drainage modeling.

2.3.1. Specification of coastal water levels

High water levels along coasts are a major source of flooding for urban systems in coastal floodplains. To represent coastal flood

processes in WRF-Hydro-CUFA, water levels can be specified along coasts and streams as surface water heads that vary in space and time, similar to the implementation in the GSSHA model (e.g., Karamouz et al., 2017; Silva-Araya et al., 2018). Given the controlled boundary for coastal water levels as specified in Fig. 2a, for example, Fig. 2b and c show subsequent floodwater spreading to neighboring intertidal wetlands at water levels of Mean Higher High Water (MHHW) and Mean Sea Level (MSL), respectively. The modeling approach provides portability and flexibility to leverage water levels from other flood-related resources, such as nearby tide gauges, regional-scale ocean hydrodynamic model simulations (e.g., Park et al., 2022 for the northern coasts of U.S. Georgia), and real-time measurements from a hyper-local sensor network (e.g., Smart Sea Level Sensors, n.d. along the U.S. Georgia coasts). The specifications of water levels can extend to coastal rivers and creeks in an estuary where coastal and fluvial flood processes are little distinctive. In addition, most ocean hydrodynamic models can solve flows further along coastal channels (Santiago-Collazo et al., 2019), which allows WRF-Hydro-CUFA to make use of the regional-scale results in a subsequent manner.

2.3.2. Coupling of WRF-Hydro and SWMM

A one-dimensional hydraulic flow solver for stormwater drainage, SWMM (version 5.1), is coupled within the routing module for overland flow in WRF-Hydro-CUFA. The coupling is made by running SWMM and exchanging the floodwater information at a regular time interval (e.g., 1-minute) during overland flow routing. At every coupling time interval, changes in the ponded water depths of stormwater inlets for one grid cell area are added to the overland flow depths at the locations of stormwater inlets. In addition, the net flow rates of stormwater outfalls are used to calculate the changes in the overland flow depths at the corresponding locations. Conversely, the updated depths of overland flows feed back into the initial and time-varying tailwater conditions of stormwater drainage components in SWMM. Then, SWMM solves the fully unsteady, explicit, dynamic wave formulation for drainage flows. The exchange of floodwater information occurs via the input and output files of SWMM, which corresponds to the loosely-coupled technique as classified by Santiago-Collazo et al. (2019).

As stormwater drainage components can exist across the decomposed computational domains for overland flow by the MPI parallelization, Noh et al. (2018) implemented the hybrid parallelization technique where the main MPI processor runs a hydraulic flow solver for all the drainage components with the Open Multi-Processing (OpenMP)

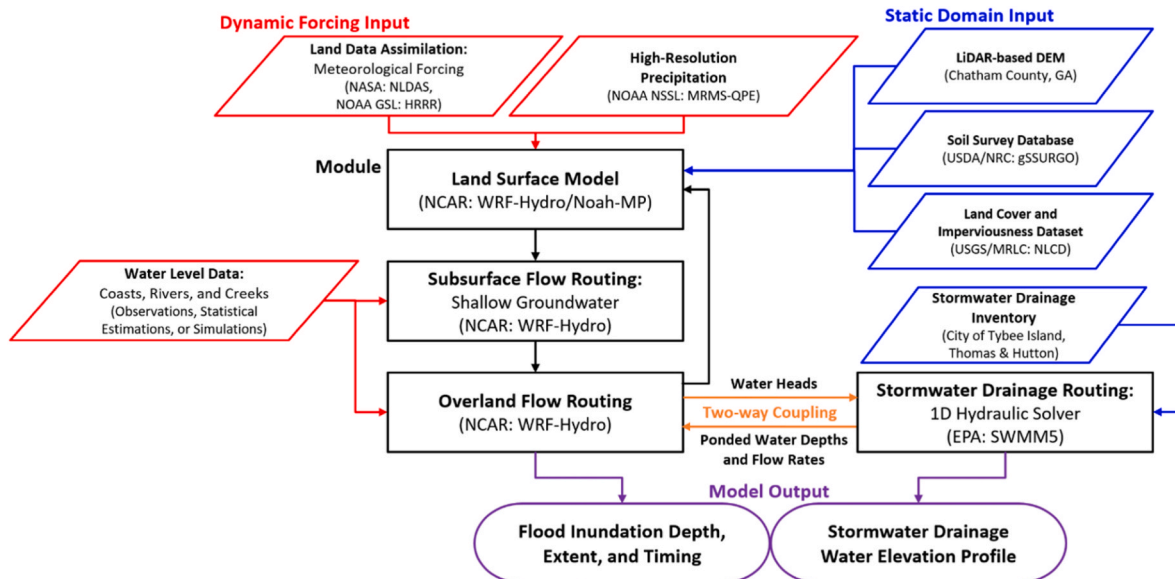


Fig. 1. Flowchart of WRF-Hydro-CUFA.

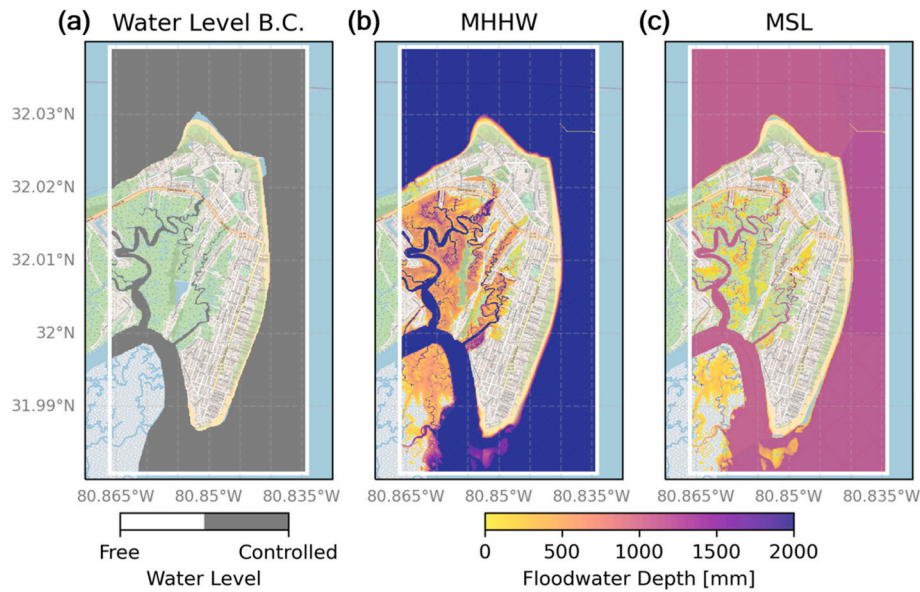


Fig. 2. Coastal water level boundary and example flooding: (a) controlled boundary for spatially- and temporally-varying water levels and (b, c) floodwater spreads at water levels of Mean Higher High Water (MHHW) and Mean Sea Level (MSL), respectively.

parallelization. For a large number of stormwater drainage components, the use of OpenMP can still be a potential bottleneck for scalability as the effective number of available OpenMP threads is limited by the number of processors in a shared memory system. To maintain the scalability of the MPI parallelization, WRF-Hydro-CUFA supports running multiple SWMM instances simultaneously on different MPI processors, each for an independent partition of stormwater drainage, and broadcasting the simulation results across the decomposed computational domains for overland flow. As study areas expand with the addition of new MPI processors, more stormwater drainage networks can be allocated to the remaining MPI processors, as illustrated in Fig. 3.

2.4. Pilot study area

The City of Tybee Island is a major tourism hub that supports the local economy and is one of the most flood-prone coastal cities in the U. S. Georgia. As shown in Fig. 4, the island is located on a coastal plain in the northernmost region of the Georgia coasts. It is surrounded by sandy beaches and dunes on the eastern shores to the Atlantic Ocean and intertidal wetlands on the western shores. While a hurricane can induce a storm surge that overtops the beach dunes on the eastern shores, most floods occur with high tides that flow into the flat, low-lying topography (light blue contours) along tidal marshes on the western shores. Particularly, the southwestern portions of the island are prone to flooding by spring tides and intensive rainfalls as these low-lying areas were developed on tidal marshes that were filled with poorly drained

soils (Evans et al., 2016). In Fig. 4, additional markers on the map depict the locations of stormwater drainage components. Most of the stormwater outfalls are located on the low-gradient lands adjacent to intertidal wetlands on the western shores, which makes the drainage capability highly subject to water levels at the outfalls.

The nearest tide gauge station is located about 6 km northwest at Fort Pulaski on the Savannah River mouth to the Atlantic Ocean, as denoted by a location marker on the map. Long-term observations of the mean sea level indicate increasing trends and accelerating rates in recent decades (Evans et al., 2016). As a result, multiple sections of U.S. Highway 80 are more frequently inundated by high tide flooding, which disrupts the transportation network and emergency responses by blocking the only access to Tybee Island. Furthermore, the following locally-observed flood threats have been a growing concern during past high tide flood events (Evans et al., 2016):

- High tides diminish the drainage capability of local stormwater infrastructure, increasing a risk of flash flooding with less extreme rainfalls.
- Saltwater occasionally flows backward from stormwater outfalls to inlets during high tides, which causes inland inundation even on sunny days.

2.5. Model input data

The flowchart of WRF-Hydro-CUFA in Fig. 1 also illustrates the

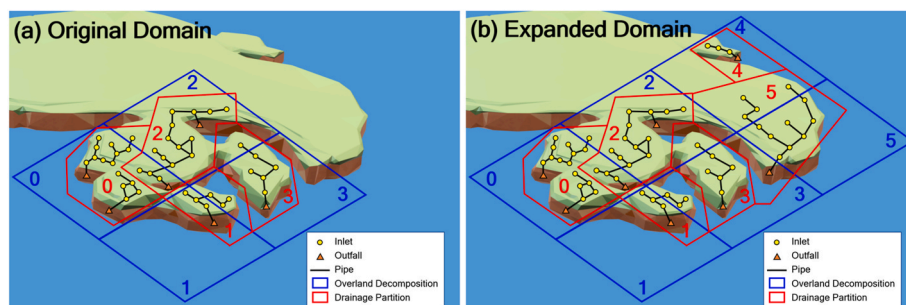


Fig. 3. 2D overland domain decomposition (blue) and 1D stormwater drainage partitions (red) as study areas expand: (a) original domain with 4 MPI processors; (b) expanded domain with 6 MPI processors. The number labels indicate the MPI ranks.

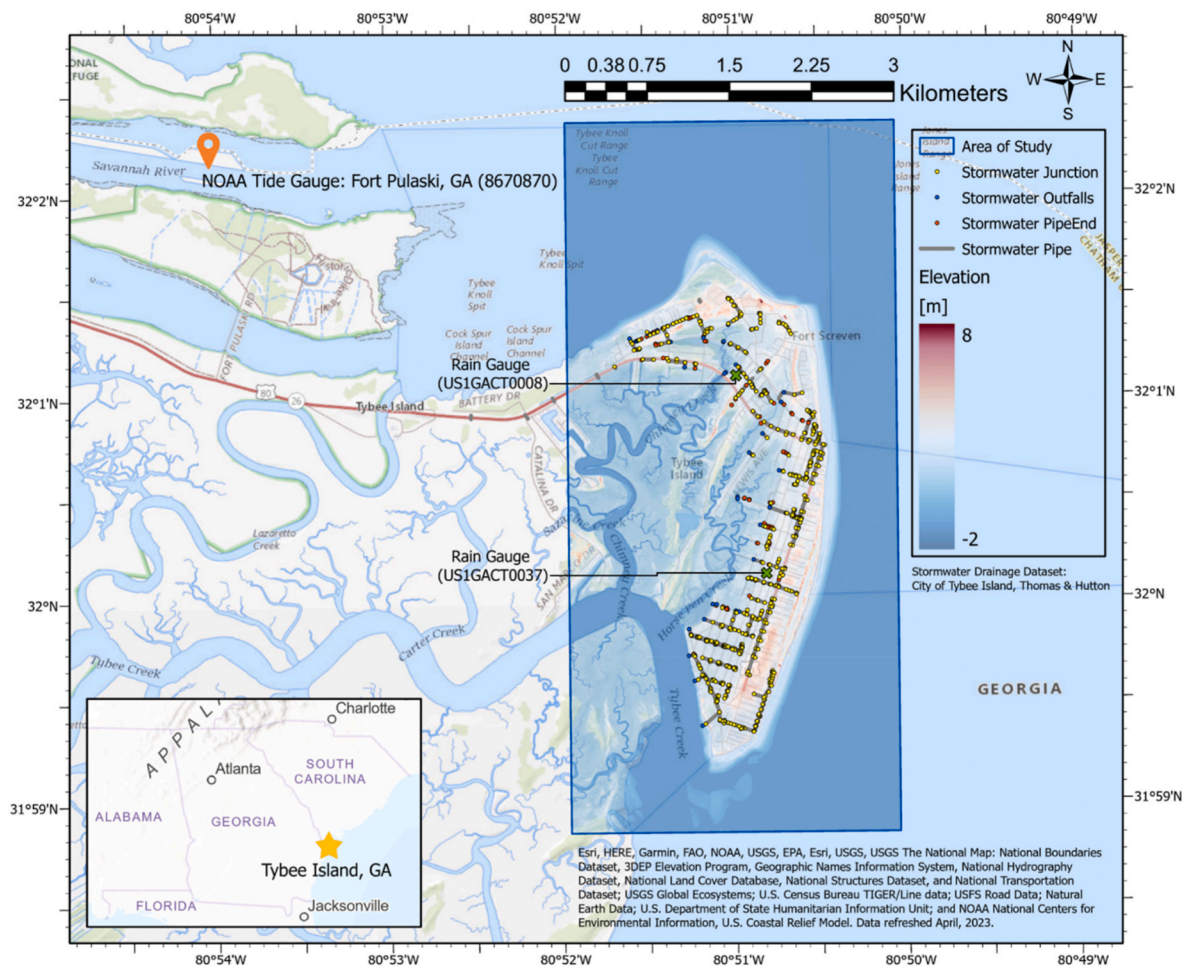


Fig. 4. Map, elevations, and stormwater drainage of the City of Tybee Island in GA, USA, with the nearest tide gauge at Fort Pulaski and two rain gauges.

required model input data of static domain and dynamic forcing for the WRF-Hydro and SWMM models. The spatially-distributed datasets of topography, soil survey database, and land characteristics are necessary as static domain inputs to parameterize numerous hydrologic variables for the modules of WRF-Hydro. In this study, the topographic elevations are obtained for 10-m hyper-resolution structured grids that span a 19.5 km^2 area, based on the LiDAR-based Digital Elevation Model of 1-m native resolution (NOAA OCM Partners, 2012). The USGS National Land Cover Database (NLCD) (Wickham et al., 2021) is used for the mapping of land parameters with the USGS 24-Type Land Covers (Loveland et al., 1995) and corresponding hydraulic roughness coefficients (Vieux, 2001). Similarly, the soil classifications are assigned from the USDA Gridded Soil Survey Geographic (gSSURGO) (Soil Survey Staff, n.d.) database into the USGS State Soil Geographic (STATSGO) (Miller and White, 1998) database with the soil hydraulic parameters (Cosby et al., 1984). Both the NLCD and gSSURGO datasets are available at the finest 30-m resolution. After the mapping by category, we adjust some of the hydrologic variables that can be directly derived from the original datasets, including infiltration parameters based on the NLCD Land Imperviousness product and saturated hydraulic conductivity of the gSSURGO database. It is assumed that the hydraulic gradients at the bottom of the soil columns be marginal, based on the local observations of poorly drained soils at the deeper soil columns. Other hydrologic properties are not modified to better understand the model capability with the initial setup before model calibrations. Along with the hydrologic variables for lands, the locations and dimensions for stormwater drainage components are needed to model stormwater inlets, pipes, and outfalls for SWMM. In our study, the surveyed inventory of stormwater

drainage serves as a basis for the flood model inputs. Similarly, the hydraulic parameters, such as pipe roughness, are set to the default values of SWMM. Given that the inventory consists of more than 1000 components, 22 independent partitions of stormwater drainage are set up based on outfalls to run simultaneously on 22 MPI processors.

For the dynamic forcing inputs, different meteorological products are implemented depending on the flood prediction modes. For past flood events, the North American Land Data Assimilation System Phase 2 (NLDAS-2) (Xia et al., 2012a, 2012b) products are combined with the Multi-Radar/Multi-Sensor System (MRMS) Quantitative Precipitation Estimation (QPE) (Zhang et al., 2016) of 1-km resolution to reflect spatially-distributed precipitation in high-resolution. For operational flood predictions on a web-based dashboard, on the other hand, the NOAA High-Resolution Rapid Refresh (HRRR) (Dowell et al., 2022; James et al., 2022) forecasts that have 3-km resolution are adopted for all the meteorological forcing variables, including precipitation. WRF-Hydro-CUFA requires an additional forcing input to impose coastal water levels as surface water heads with respect to space and time. We use the controlled boundary of coastal water levels shown in Fig. 2a to potentially leverage water level outputs from a water level monitoring network (Smart Sea Level Sensors, n.d.) and regional-scale model forecasts (CMCC, n.d.). Due to the lack of information on historical water level variability along the coastlines, our study assumes that water levels be spatially uniform over the controlled boundary. The time series of water levels are obtained from the nearest tide gauge at Fort Pulaski based on observations (NOAA, n.d.-b) for past flood events and hydrograph forecasts (NOAA NWS, n.d.) for operational flood predictions, respectively. As the meteorological forcing inputs are currently on an

hourly basis, the water level inputs are linearly interpolated to the hourly time intervals.

2.6. Model spin-up

The applications of hydrologic models require a sufficient period of model spin-up to allow reaching model equilibrium states. The determination of adequate spin-up durations depends on various factors, including the model components, scales, and watershed characteristics (Seck et al., 2015). For WRF-Hydro, model spin-up periods of more than one month have been applied to simulate streamflow flood discharge in river basin scales (Lin et al., 2018; Zhang et al., 2020). Given that coastal-urban scales for hyper-resolution modeling are significantly smaller compared to river basin scales, we consider that spin-up periods over two weeks are generally sufficient for flood applications in coastal-urban systems. Nevertheless, the spin-up durations need to be further extended to include antecedent events that may influence soil moisture conditions.

3. Model simulations for past flood events

WRF-Hydro-CUFA aims at the broad applications of flood predictions not only for hurricane-induced storm surges but also nuisance floods that are driven by different flood mechanisms in coastal-urban systems. Therefore, our study chooses two representative flood events, one non-extreme and one extreme, for simulations. The first application is for the perigean spring tides in November 2012, which flooded the southwestern portions of the City of Tybee Island directly and through stormwater drainage with concurrent rainfalls (Section 3.1). The flood event in November 2012 is selected because the flood extents and corresponding geo-referenced photos are well-documented by Evans et al. (2016). The second application is for Hurricane Irma in September 2017, which led to extensive inundation on most of the island due to high storm tides and heavy rainfalls (Section 3.2).

3.1. Non-extreme flood event: perigean spring tide in November 2012

During the perigean spring tide in November 2012, the elevated water levels triggered flooding in the flat, low-lying areas of the island. In Fig. 5a, the observations of water levels (blue line) at the Fort Pulaski tide gauge (NOAA, n.d.-b) show that the tidal peaks of similar amplitude repeated four times as denoted by star markers. In addition, the daily measurements of precipitation (red line) at the local rain gauge (US1GACT0008) (NOAA NCEI, n.d.) indicated the simultaneous occurrence of rainfalls during the high tides of the second peak. During the tidal peaks, Evans et al. (2016) identified flooding at two different locations (red ellipses) as shown in the inset photos of Fig. 5b. Across the coastlines on the western shores, the high tides directly overtopped the coastal banks adjacent to the tidal marshes, which led to flooding along the street on the coastal banks. At the same time, the submerged stormwater outfall (circle marker with label A) allowed saltwater to flow back through the corresponding pipe (black line) and overflow at some of the inlets (circle markers with label B to Q) where the elevations are relatively low.

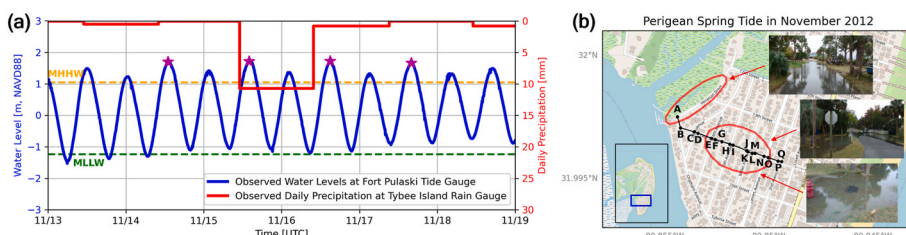


Fig. 5. Flooding due to overtopping and stormwater backflows during perigean spring tides in November 2012: (a) water levels (blue) at the Fort Pulaski tide gauge and daily precipitation (red) at the local rain gauge (US1GACT0008). The star markers indicate the four repeating tidal peaks of similar amplitude; (b) flood extents (red ellipses) and photos identified in Evans et al. (2016). The black line and circles represent the relevant stormwater pipe, inlets (label B to Q), and outfall (label A), respectively. Inset photos: Courtesy of Evans et al. (2016).

The flood simulations using WRF-Hydro-CUFA have been performed to demonstrate the capability to represent multiple flood mechanisms, including high tide flooding along coasts and through stormwater drainage and its compounding effects with pluvial processes. The model run is set to begin on October 31, which covers the previous rainfall event from November 05 to 07. Using 48 CPU cores, about 2.5 wall-clock hours are required for the 21-day simulation. In Fig. 6, each panel shows the floodwater depths and corresponding elevation profile of the stormwater drainage section at 1 hour after each tidal peak, respectively. Particularly, the stormwater elevation profile contains both the water elevations (blue line with underneath shade) and ground elevations (green line) for the inlets and outfall, which implies that flooding occurred at the inlets (label color in red) where the water elevation exceeds the ground elevation. Compared to the first inset photo of Fig. 5b, all the results of flood extents similarly show direct inundation along the street on the coastal banks, which are roughly analogous to one another as the tidal peaks are virtually identical. In addition, the developed flood model predicts inland inundation in the surrounding areas of the stormwater inlets due to the overflow as shown in the second and third inset photos of Fig. 5b. However, the results indicate more extensive flooding for the second tidal peak (Fig. 6b) in comparison to those for the other tidal peaks (Fig. 6a, c, and d). The increases in flood depths and extents are due to the coincidence of the storm rainfalls during the second tidal peak. In other words, the high tides induced the stormwater drainage to be overwhelmed with flooding, eventually blocking the drainage of the rainfall-runoff. As a result, the stormwater elevation profile in Fig. 6b exhibits a greater number of stormwater inlets with flooding as highlighted in red more on the inlet letter labels. During the second tidal peak, the increases in the floodwater depths due to the concurrent rainfalls are obvious for the stormwater inlets located in low elevations.

Concerns about flooding prompted the city to install backflow preventers to avert saltwater encroachment and subsequent stormwater flooding in low-lying areas (Evans et al., 2016). As a hypothetical scenario, the simulations with a backflow preventer retrofitted have been conducted for the same flood event. Similarly, the panels in Fig. 7 show the flood depths, extents, and corresponding stormwater elevation profiles. Compared to those in Fig. 6, no changes are identified for floodwater that directly overtopped the coastal banks. Instead, the results for the hypothetical scenario show that the retrofit of a backflow preventer ideally eliminates the occurrence of saltwater backflows (Fig. 7a). During the second tidal peak (Fig. 7b), however, a flood risk persists as the rainfall-runoff causes flash flooding around the lowest-lying stormwater inlets (labels E, I, and N).

3.2. Extreme flood event: Hurricane Irma in September 2017

Hurricane Irma in September 2017 is one of the major hurricanes that inflicted extensive damage on the City of Tybee Island. During the hurricane's landfall as illustrated in Fig. 8, it produced a storm surge that caused the maximum flood depths of 0.9 m–1.5 m along the Georgia coasts with the total precipitation between 120 mm and 250 mm (Cangialosi et al., 2018). As shown in Fig. 8b, particularly, the peak storm tide (blue line) was as high as 1.4 m above MHHW at the Fort Pulaski

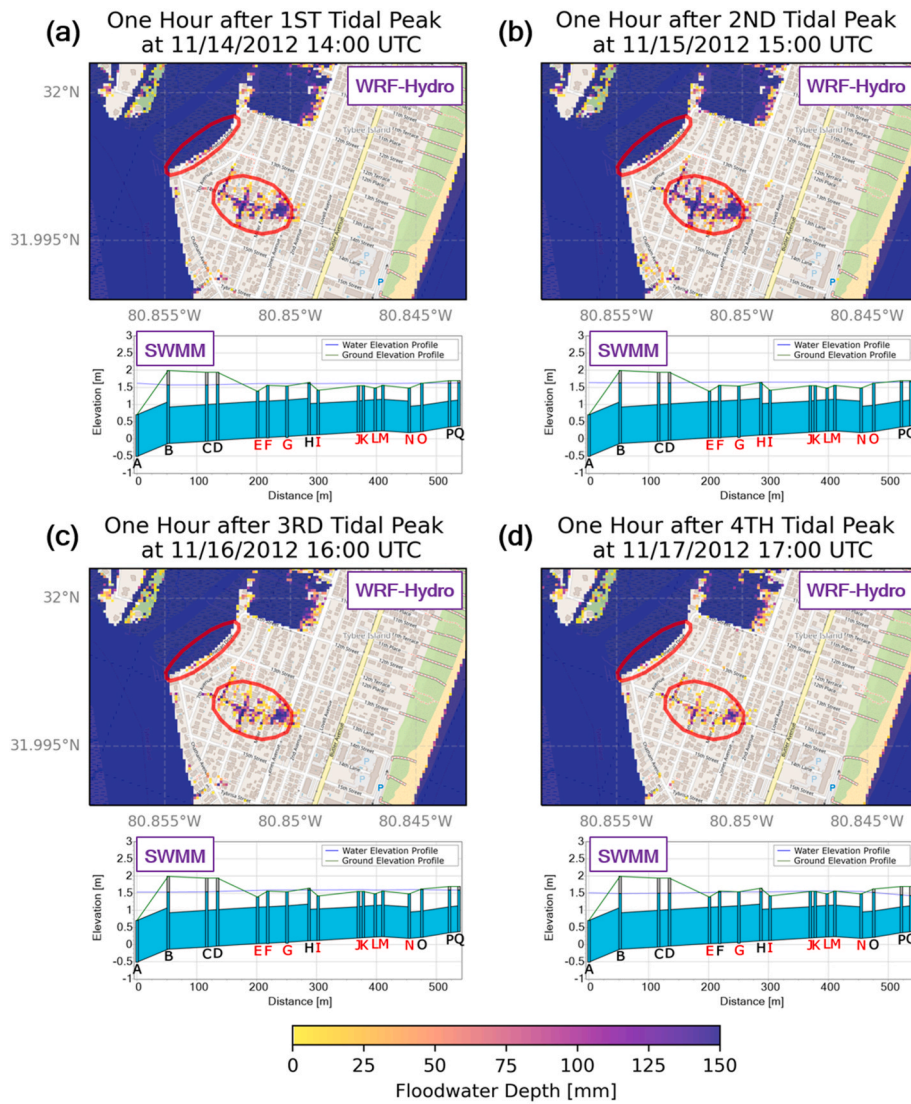


Fig. 6. Simulated floodwater depths and corresponding elevation profile of the stormwater pipe at 1 hour after each tidal peak. The red ellipses in Fig. 5b are added for comparison of the flood extents. In each elevation profile, the letter labels in red indicate the flooded inlets where the water elevation is higher than the ground elevation. The locations of the stormwater inlets and outfall (letter labels) are shown in Fig. 5b.

tide gauge (NOAA, n.d.-b) while the precipitation (red line) at the local rain gauge (US1GACT0037) (NOAA NCEI, n.d.) exceeded 135 mm in two days. As a result, a combination of coastal and pluvial processes led to compound flooding in many urban areas of the island. As noticeable rainfall events occurred multiple times within a few weeks before the hurricane's landfall, the flood simulations with WRF-Hydro-CUFA cover the periods more than a month before to spin up properly as a hydrologic flood model. It takes about 8.5 wall-clock hours for 48 CPU cores to run the 77-day simulation.

At the peak storm tide, as shown in Fig. 9a, the resulting flood depths and extents show extensive inundation across the island. Notably, the extreme water levels severely flooded the neighboring low-gradient lands of the coastal creeks and marshes on the western shores, including the southwestern portions of the island that have limited drainage capabilities. Fig. 9b compares the simulated water levels with the USGS measurements of storm tides and nearby high-water marks (USGS, n.d.) at the upland locations (triangular markers in Fig. 9a). In the plots, it should be noted that the flat parts of the water levels represent the minimum water elevations for records, namely the sensor elevations for the USGS loggers and the ground elevations for the flood model, respectively. For example, the USGS sensors were attached to

vertical structures, such as tree trunks and bridge abutments, which requires floodwater to reach the sensor elevations to provide actual readings. For the water levels that exceeded the USGS sensor elevations, the simulation results (blue line) reproduce the temporal evolutions of floodwater by adequately capturing the rising and falling trends. In addition, although no exact time information exists for the USGS high-water marks, the simulated peaks of water levels match closely with the surveyed ones at the corresponding locations.

We carry out further comparisons at the level of individual streets. Owing to the absence of recorded flood data in inland urban areas, the comparisons are achieved by utilizing soft data based on flood image datasets, which were gathered from the internet, as shown in Fig. 9c. For instance, one of the datasets is aerial footage that was taken from a helicopter by the mayor of the City of Tybee Island at that time right after the hurricane hit the island (Buelterman, 2017). In addition, the datasets include on-site photos and videos that captured the instances of flooding by the local broadcasts and residents (McDaniel, 2017a, b; WTOC, 2017a, b; Jarvis, 2017; Galloway, 2017). After identifying the geographic locations of the collected images, our study compares the overall severity of flooding with the simulation results (contour overlay) at different locations on the map in Fig. 9c. For example, the second inset

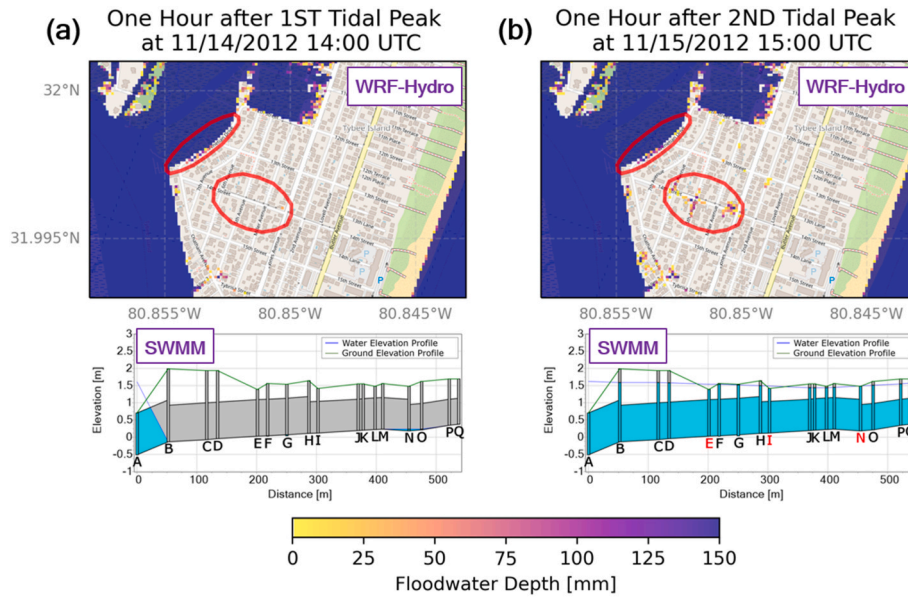


Fig. 7. Same simulations as Fig. 6, but hypothetically retrofitting a backflow preventer to the stormwater outfall (letter A). Similarly, in each elevation profile, the letter labels in red imply flooding at the stormwater inlets. In the elevation profile in (a), no water exists between outfall A and inlet B, although it appears graphically when connecting the two water elevations.

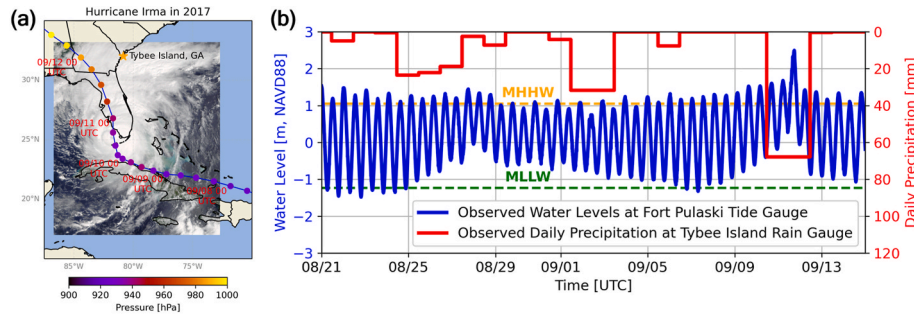


Fig. 8. Hurricane Irma in September 2017: (a) hurricane track with intensity and (b) water levels (blue) at the Fort Pulaski tide gauge and daily precipitation (red) at the local rain gauge (US1GACT0037). Satellite image credit: Schmalz et al. (2017).

photo in the top row shows that floodwater flowed with curb-height depths (0.15–0.20 m) along U.S. Highway 80, which is consistent with the shallow-depth flooding (<0.25 m; light yellow contours) on the map. Both the flood simulation map and reported images indicate severe, extensive inundation (>0.7 m; purple contours) in the surrounding residential areas of the wetlands, as shown in the photos in the left column. Furthermore, in the eastern parts where elevations are relatively higher, localized flooding driven by the intensive rainfalls and dune-overtopping flows are identified by both the information, with limited depth (less than 0.5 m) in the topographically-depressed areas (the first and second photos in the right column) and via the beach access (the third photo in the same column).

4. Model application for operational flood predictions

Our study extends an application of WRF-Hydro-CUFA into a prototype operational flood prediction system via a web-based dashboard, which currently runs for the City of Tybee Island as a pilot study (Fig. 10; <https://tybee.cos.gatech.edu>). To provide flood predictions for the next three days, the Linux bash scripts are executed at each forecast cycle (e. g., 6- or 12-hour) to process the dynamic forcing inputs, run the flood model simulations, and upload the inputs and results into a server that hosts a web-based dashboard. Accordingly, the dashboard first displays the hydrologic simulation results for flood predictions (Fig. 10a), such as

floodwater depths and approximate soil saturation depths. In addition, it exhibits the modeling data of meteorological forcing (e.g., precipitation) and static domains (e.g., elevations, land parameters, and soil textures), as shown in Fig. 10b and c, respectively. Furthermore, the platform integrates other relevant resources to floods, including real-time feeds from web and traffic cameras (Fig. 10d), water level measurements from nearby tide gauges and hyper-local sensors (Fig. 10e), and a link to a map-based archive for past flood photos and videos (Fig. 10f). Consequently, the platform provides users integrated access to flood predictions, modeling data, and real-time footage, facilitating enhanced understandings and assessments of the model prediction skills.

5. Discussion

Coastal communities face a growing risk of flooding due to sea level rise and subsequent impacts on stormwater drainage systems. The flood threats are an urgent problem in low-lying areas with flat topography, impermeable grounds, and thin unsaturated soil layers. Based on the WRF-Hydro and SWMM models, our study develops WRF-Hydro-CUFA to better capture the complex dynamics of floodwater interacting with natural and engineered drainage in coastal-urban systems.

The model simulations of nuisance flooding (Section 3.1) can reproduce the reported flood mechanisms, directly over coastal banks and through stormwater drainage, during the perigean spring tides.

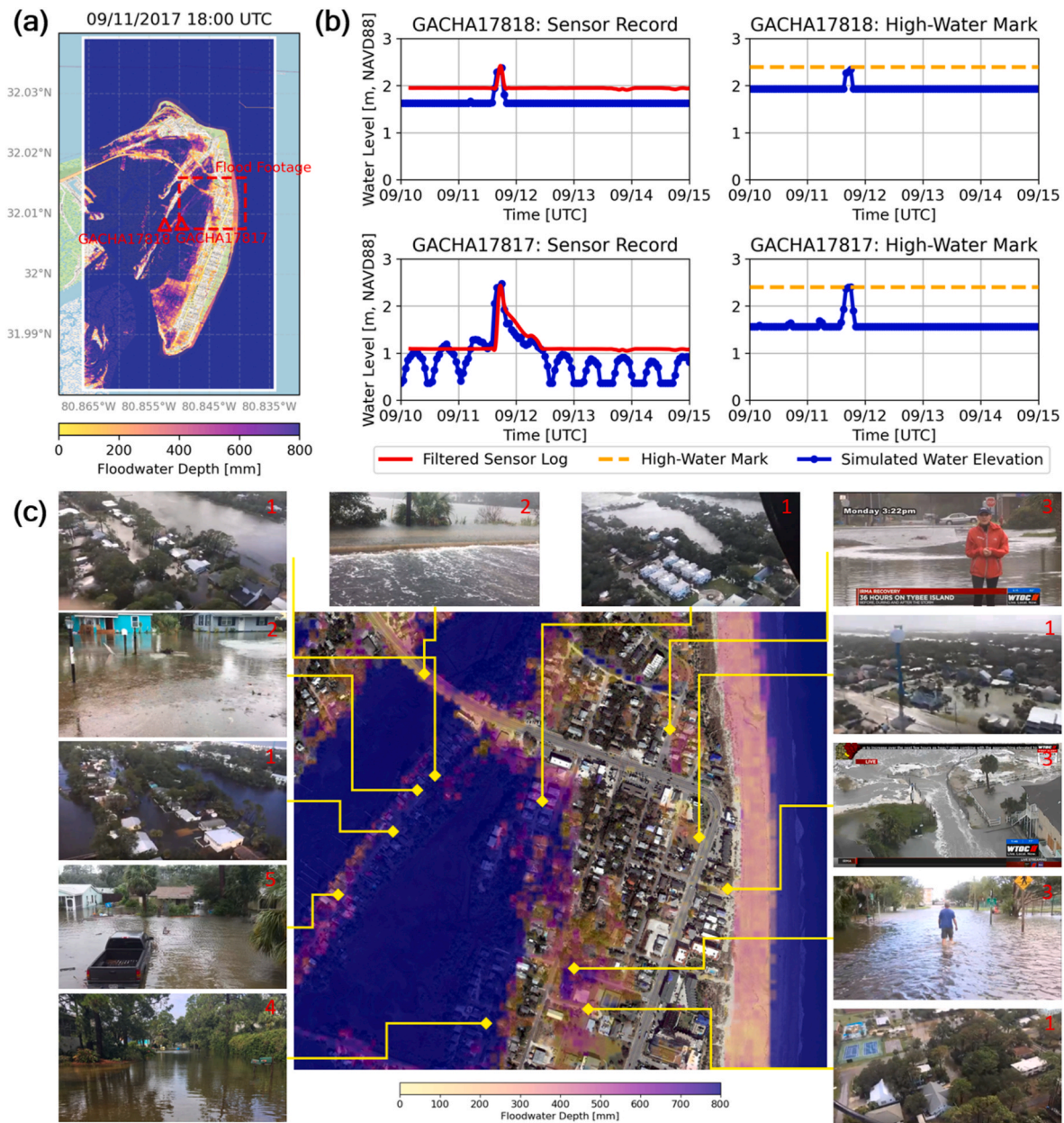
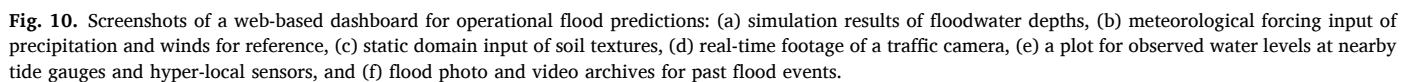


Fig. 9. Simulated flood information and comparisons with the observations: (a) floodwater depths at the highest storm tide and locations of the observations (red), (b) validations with the USGS sensor logs and nearby high-water marks, and (c) comparisons with the flood images collected from the internet. Inset image credits: 1 – Buelterman (2017), 2 – McDaniel (2017a, 2017b), 3 – WTOC (2017a, 2017b), 4 – Jarvis (2017), 5 – Galloway (2017).

Moreover, the flooding adjacent to low-lying inlets becomes distinctively extensive during the tidal peak occurring concurrently with the storm rainfalls, which demonstrates the model capability to represent compound flooding of high tides and rainfalls. The flood extents indicate that the surrounding areas of low-lying stormwater inlets are more vulnerable to compound flooding despite the proximity to the inlets, particularly when stormwater systems become overwhelmed. This is because stormwater inlets are typically constructed on relatively low topography, such as depressed lands, to collect rainfall-runoff that naturally flows over terrain by gravity. The identical simulations with a retrofitted backflow preventer show that the high tailwater conditions at the stormwater outfall significantly diminish the drainage capability by blocking the discharge of the rainfall-runoff into the coasts. These results are consistent with those found by Shen et al. (2019) that examined flood reduction effects of outfall flap gates for a combined scenario of rainfalls and storm tides. Therefore, while a backflow preventer is often

proposed as a measure to mitigate saltwater penetration through stormwater drainage in response to sea level rise, a risk of flash flooding still exists due to the prolonged exposure to high tailwater conditions that strain the drainage capability in coastal-urban systems. These concerns are increasingly widespread among coastal communities, particularly in underserved communities (National Academies, 2019).

For Hurricane Irma (Section 3.2), the comparisons of the flood depths with the USGS records show that the model simulations reasonably represent not only the peak flood levels but also the proceeding, receding, and infiltration processes of floodwater based on the hydrologic and hydraulic modeling of coastal-urban systems. Particularly, the USGS sensor records (GACHA17817 in Fig. 9b) are an important indicator for model representations of hydrologic and hydraulic processes as the storm tide sensor was located near the upstream wetlands that are interconnected by culvert pipes. During Hurricane Irma, excessive water flowing from the wetlands inundated the adjacent



In this study, we further apply WRF-Hydro-CUFA in a web-based dashboard that consists of operational flood predictions, modeling information, and existing flood-related resources, such as real-time camera feeds and nearby water level measurements. The dashboard allows public and emergency officials to beta-test short-term flood predictions to identify local flood threats and make informed decisions about emergency preparedness, particularly for compound flood events of high tides and heavy rainfalls. The participation of community officials can lead to further research and co-design with local stakeholders, which is necessary to apply the flood model and operational predictions as a part of emergency management systems. For flood modeling researchers, the platform provides an opportunity to consistently manage the flood model with monitoring and to collaborate with other researchers and practitioners who are knowledgeable about site-specific flood characteristics. For example, the integration of real-time camera feeds enables direct comparisons of the flood model predictions with the on-site situations, which contributes to understanding model performances and limitations. The modeling inputs that are simultaneously available on the same platform can help identify existing knowledge gaps in flood modeling and potentially reduce inherent uncertainties of the inputs and dynamics through model calibrations. In addition, the flood model enhancements can be achieved by collaboration with local experts who may share detailed survey datasets or site-specific understandings of past flood events. Through long-term improvements

5.1. Limitations

The presented results in this study have various sources of

uncertainties, such as model inputs, assumptions, calibrations, and validations. Although the flood model simulations are performed in 10-m hyper-resolution, the hydrologic properties for lands and soils are derived based on the 30-m resolution NLCD and gSSURGO datasets. In addition, modeling gaps may arise when remapping these datasets into the USGS 24-Type Land Covers and STATSGO datasets. Furthermore, coastal communities may lack access to hyper-resolution datasets sufficient to represent lands and soils. The limited representation of fine-scale urban terrain and features results in inaccuracies in predicting flood depths and extents (Wang et al., 2018). Hence, model users should be careful with flood predictions by the initial model setup based on coarse-resolution datasets and focus more on calibrations to reduce the model uncertainties. For example, the initial modeling gaps in model input datasets may be reduced by combining with remote sensing and localized surveys, as implemented by Hossain Anni et al. (2020).

Our study currently applies a time series of uniform wave levels obtained from the nearest tide gauge. As water levels in an estuary show complex patterns due to the interactions with atmospheric forcing and local landscapes, the simplified approach can result in inaccurate estimations of the flood depths and extents (Gallien et al., 2011), particularly during hurricane-induced flood events. To address such challenges, future research should couple the flood model into other simulation (e.g., CMCC, n.d.; Louisiana State University, n.d.) or observation (e.g., Smart Sea Level Sensors, n.d.; NOAA, n.d.-a) frameworks in a subsequent manner to consider the effects of water level variability on flooding.

The comparisons of street-scale inland flooding are based on the collected flood images, which provide no statistical measure for confidence levels. Currently, there are no high-quality measurement datasets available across the flooded sites during Hurricane Irma. A paucity of observation datasets across flooded areas inhibits the assessment of urban flood modeling (Gallien et al., 2018). Therefore, further comprehensive calibrations and validations should be taken to better understand the model prediction skills, which may be based on the integrated platform for operational predictions.

6. Conclusions

WRF-Hydro-CUFA is an open-source flood modeling extension to WRF-Hydro for hyper-resolution coastal and urban applications, with an aim of providing an accessible option for coastal communities to assess emerging flood risks. It is built based upon a distributed process-based hydrologic model, WRF-Hydro, to adequately represent hydrologic processes in a heterogeneous urban setting. In WRF-Hydro-CUFA, water levels along coasts and rivers can be specified based on observations, statistical estimations, or regional-scale simulations, which can provide flooding mechanisms due to high water levels. Moreover, it has a function to couple with a hydraulic flow solver for stormwater drainage, SWMM, to take account of floodwater redistribution by stormwater drainage in the built environment. Therefore, the developed flood model can serve as an advanced tool for understanding hydrologic and hydraulic characteristics of flooding in coastal-urban systems, which can

narrow modeling gaps attributed to common assumptions, such as impervious land and ineffective stormwater drainage. The simulations for past flood events demonstrate the model applicability, ranging from nuisance floods to hurricane-induced floods. Moreover, the flood model is capable of being deployed to run in operation modes, which will contribute to strengthening the model robustness and supporting localized strategies for flood resilience by readily adapting to ongoing urban developments. Ultimately, the application, monitoring, enhancement, and adaptation processes can be transferred to other coastal communities at a higher risk of flooding.

Code availability

The source codes for the WRF-Hydro (Gochis et al., 2020) and SWMM (Rossman, 2015) models are open and publicly available with documentation at the following websites, respectively:

- NCAR RAL WRF-Hydro: https://ral.ucar.edu/projects/wrf_hydro
- EPA SWMM: <https://www.epa.gov/water-research/storm-water-management-model-swmm>

The modified codes for WRF-Hydro-CUFA are openly available in the following GitHub repository with descriptions and usages: <https://github.com/angjuny/WRF-Hydro-CUFA>.

Data availability

The input data of coastal water levels and meteorological forcing can be found in the indicated references, respectively. The flood simulation data can be provided upon request to the corresponding author (Y. Son).

Declaration of competing interest

The authors declare that they have no known competing financial interests or personal relationships that could have appeared to influence the work reported in this paper.

Acknowledgments

This research is funded by the NOAA Coastal Infrastructure and Resilience Research Initiative: The Georgia Coastal Equity and Resilience (CEAR) Hub project (NA22NOS4690219). We would like to thank Alan Robertson of the City of Tybee Island, Dr. Clark Alexander, Dr. Brian Bledsoe, Jill Gambill at the University of Georgia, and Kevin Smith of Thomas & Hutton for gratefully providing the stormwater drainage survey data, helping in identifying the geographic locations of flood photos, and sharing invaluable experiences from past flood events in the City of Tybee Island. We also wish to thank Dr. Jason Evans at Stetson University, Jason Buelterman, and WTOC for granting permission to use flood images in this research. We thank the anonymous reviewers for providing thoughtful and constructive feedback.

Appendix A

WRF-Hydro input parameter for the decay coefficient of the infiltration capacity

WRF-Hydro uses an input parameter, K_{dref} , to scale the decay coefficient, k , of the infiltration capacity in Eq. (2):

$$k = K_{dref} \times \frac{K_{sat}}{K_{ref}} \quad (A.1)$$

where K_{sat} is saturated hydraulic conductivity and K_{ref} is its reference value (e.g., saturated hydraulic conductivity for silty clay loam). In this study, the NLCD Land Imperviousness datasets (Wickham et al., 2021) are used to derive K_{dref} , which is shown in Fig. A.1.

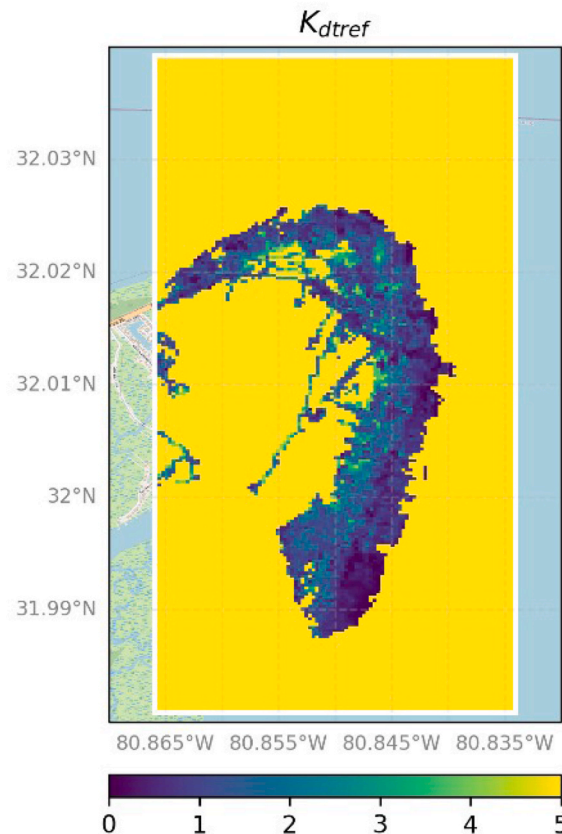


Fig A.1. WRF-Hydro input parameter, K_{dref} , for infiltration.

References

- Blumberg, A.F., Georgas, N., Yin, L., Herrington, T.O., Orton, P.M., 2015. Street-scale modeling of storm surge inundation along the New Jersey hudson river waterfront. *J. Atmos. Ocean. Technol.* 32 (8), 1486–1497. <https://doi.org/10.1175/jtech-d-14-00213.1>.
- Bosserelle, A.L., Morgan, L.K., Hughes, M.W., 2022. Groundwater rise and associated flooding in coastal settlements due to sea-level rise: a review of processes and methods. *Earth's Future* 10 (7). <https://doi.org/10.1029/2021ef002580>.
- Buchanan, M.K., Kulp, S., Cushing, L., Morello-Frosch, R., Nedwick, T., Strauss, B., 2020. Sea level rise and coastal flooding threaten affordable housing. *Environ. Res. Lett.* 15 (12). <https://doi.org/10.1088/1748-9326/abb266>.
- Buelterman, J., 2017. Flying to tybee from thunderbolt: facebook. <https://www.facebook.com/jason.buelterman/videos/1104252633042272/>.
- Cangialosi, J.P., Latto, A.S., Berg, R., 2018. Tropical Cyclone Report: Hurricane Irma. AL 112017. National Hurricane Center. https://www.nhc.noaa.gov/data/tcr/AL112017_Irma.pdf.
- Chen, W., Huang, G., Zhang, H., Wang, W., 2018. Urban inundation response to rainstorm patterns with a coupled hydrodynamic model: a case study in Haidian Island, China. *J. Hydrol.* 564, 1022–1035. <https://doi.org/10.1016/j.jhydrol.2018.07.069>.
- Clapp, R.B., Hornberger, G.M., 1978. Empirical equations for some soil hydraulic properties. *Water Resour. Res.* 14 (4), 601–604. <https://doi.org/10.1029/WR014i004p00601>.
- CMCC, n.d. Savannah - water integrated tool for ocean, coastal and river hydraulics forecasting. <https://savannah.cmcc.it/>. (Accessed 17 May 2023).
- Cosby, B.J., Hornberger, G.M., Clapp, R.B., Ginn, T.R., 1984. A statistical exploration of the relationships of soil moisture characteristics to the physical properties of soils. *Water Resour. Res.* 20 (6), 682–690. <https://doi.org/10.1029/WR020i006p00682>.
- Costabile, P., Costanzo, C., De Lorenzo, G., Macchione, F., 2020. Is local flood hazard assessment in urban areas significantly influenced by the physical complexity of the hydrodynamic inundation model? *J. Hydrol.* 580. <https://doi.org/10.1016/j.jhydrol.2019.124231>.
- Dowell, D.C., Alexander, C.R., James, E.P., Weygandt, S.S., Benjamin, S.G., Manikin, G. S., Blake, B.T., Brown, J.M., Olson, J.B., Hu, M., Smirnova, T.G., Ladwig, T., Kenyon, J.S., Ahmadov, R., Turner, D.D., Duda, J.D., Alcott, T.I., 2022. The high-resolution Rapid Refresh (HRRR): an hourly updating convection-allowing forecast model. Part I: motivation and system description. *Weather Forecast.* 37 (8), 1371–1395. <https://doi.org/10.1175/waf-d-21-0151.1>.
- Downer, C.W., Ogden, F.L., 2004. GSSHA: model to simulate diverse stream flow producing processes. *J. Hydrol. Eng.* 9 (3), 161–174. [https://doi.org/10.1061/\(asce\)1084-0699\(2004\)9:3\(161\)](https://doi.org/10.1061/(asce)1084-0699(2004)9:3(161)).
- Evans, J.M., Gambill, J., McDowell, R.J., Prichard, P.W., Hopkinson, C.S., 2016. Tybee island sea-level rise adaptation plan. Georgia sea grant. <https://www.researchgate.net/publication/289999590>.
- Gallien, T.W., 2016. Validated coastal flood modeling at Imperial Beach, California: comparing total water level, empirical and numerical overtopping methodologies. *Coast. Eng.* 111, 95–104. <https://doi.org/10.1016/j.coastaleng.2016.01.014>.
- Gallien, T.W., Kalligeris, N., Delisle, M., Tang, B., Lucey, J., Winters, M., 2018. Coastal flood modeling challenges in defended urban backshores. *Geosciences* 8 (12). <https://doi.org/10.3390/geosciences8120450>.
- Gallien, T.W., Sanders, B.F., Flick, R.E., 2014. Urban coastal flood prediction: integrating wave overtopping, flood defenses and drainage. *Coast. Eng.* 91, 18–28. <https://doi.org/10.1016/j.coastaleng.2014.04.007>.
- Gallien, T.W., Schubert, J.E., Sanders, B.F., 2011. Predicting tidal flooding of urbanized embayments: a modeling framework and data requirements. *Coast. Eng.* 58 (6), 567–577. <https://doi.org/10.1016/j.coastaleng.2011.01.011>.
- Galloway, F., 2017. Hurricane Irma 2017: WTCO. <https://www.wtco.com/2019/05/30/tybee-island-recovery-efforts-continue-years-after-hurricanes/>.
- Gochis, D.J., Barlage, M., Cabell, R., Casali, M., Dugger, A., FitzGerald, K., McAllister, M., McCreight, J., RafieeNasab, A., Read, L., Sampson, K., Yates, D., Zhang, Y., 2020. The WRF-Hydro® Modeling System Technical Description (Version 5.2.0). NCAR Technical Note, p. 108. <https://ral.ucar.edu/sites/default/files/public/projects/wrf-hydro/technical-description-user-guide/wrf-hydrov5.2technicaldescription.pdf>.
- Habel, S., Fletcher, C.H., Anderson, T.R., Thompson, P.R., 2020. Sea-level rise induced multi-mechanism flooding and contribution to urban infrastructure failure. *Sci. Rep.* 10 (1), 3796. <https://doi.org/10.1038/s41598-020-60762-4>.
- Hallegatte, S., Green, C., Nicholls, R.J., Corfee-Morlot, J., 2013. Future flood losses in major coastal cities. *Nat. Clim. Change* 3 (9), 802–806. <https://doi.org/10.1038/nclimate1979>.
- Horton, R.E., 1941. An approach toward a physical interpretation of infiltration-capacity. *Soil Sci. Soc. Am. J.* 5 (C), 399–417. <https://doi.org/10.2136/sssaj1941.036159950005000C0075x>.
- Hossain Anni, A., Cohen, S., Praskievicz, S., 2020. Sensitivity of urban flood simulations to stormwater infrastructure and soil infiltration. *J. Hydrol.* 588. <https://doi.org/10.1016/j.jhydrol.2020.125028>.
- James, E.P., Alexander, C.R., Dowell, D.C., Weygandt, S.S., Benjamin, S.G., Manikin, G. S., Brown, J.M., Olson, J.B., Hu, M., Smirnova, T.G., Ladwig, T., Kenyon, J.S., Turner, D.D., 2022. The high-resolution Rapid Refresh (HRRR): an hourly updating

- convection-allowing forecast model. Part II: forecast performance. *Weather Forecast.* 37 (8), 1397–1417. <https://doi.org/10.1175/waf-d-21-0130.1>.
- Jarvis, W., 2017. Irma swapped tybee island: the atlanta journal-constitution. <https://www.ajc.com/news/breaking-news/like-matthew-irma-set-flooding-record-tybee-island/wFw2dpU3BVZwWiwXNTanJ/>.
- Joyce, J., Chang, N., Harji, R., Ruppert, T., Singhofen, P., 2017. Cascade impact of hurricane movement, storm tidal surge, sea level rise and precipitation variability on flood assessment in a coastal urban watershed. *Clim. Dynam.* 51 (1–2), 383–409. <https://doi.org/10.1007/s00382-017-3930-4>.
- Julien, P.Y., Saghaffian, B., Ogden, F.L., 1995. Raster-based hydrologic modeling of spatially-varied surface runoff. *J. Am. Water Resour. Assoc.* 31 (3), 523–536. <https://doi.org/10.1111/j.1752-1688.1995.tb04039.x>.
- Karamouz, M., Razmi, A., Nazif, S., Zahmatkesh, Z., 2017. Integration of inland and coastal storms for flood hazard assessment using a distributed hydrologic model. *Environ. Earth Sci.* 76 (11) <https://doi.org/10.1007/s12665-017-6722-6>.
- Kim, S., Shen, H.J., Noh, S., Seo, D.J., Welles, E., Pelgrim, E., Weerts, A., Lyons, E., Phillips, B., 2021. High-resolution modeling and prediction of urban floods using WRF-Hydro and data assimilation. *J. Hydrol.* 598 <https://doi.org/10.1016/j.jhydrol.2021.126236>.
- Lin, P.R., Yang, Z.L., Gochis, D.J., Yu, W., Maidment, D.R., Somos-Valenzuela, M.A., David, C.H., 2018. Implementation of a vector-based river network routing scheme in the community WRF-Hydro modeling framework for flood discharge simulation. *Environ. Model. Software* 107, 1–11. <https://doi.org/10.1016/j.envsoft.2018.05.018>.
- Liu, T., Su, X., Prigibobbe, V., 2018. Groundwater-sewer interaction in urban coastal areas. *Water* 10 (12). <https://doi.org/10.3390/w10121774>.
- Louisiana State University, n.d. Coastal emergency risks assessment: storm surge guidance for emergency management and real-time decisions. <https://cera.coastalrisk.live>. (Accessed 17 May 2023).
- Loveland, T.R., Merchant, J.W., Brown, J.F., Ohlen, D.O., Reed, B.C., Olson, P., Hutchinson, J., 1995. Seasonal land-cover regions of the United States. *Ann. Assoc. Am. Geogr.* 85 (2), 339–355. <https://doi.org/10.1111/j.1467-8306.1995.tb01797.x>.
- Marsooli, R., Wang, Y., 2020. Quantifying tidal phase effects on coastal flooding induced by hurricane sandy in manhattan, New York using a micro-scale hydrodynamic model. *Front. Built Environ.* 6 <https://doi.org/10.3389/fbuil.2020.00149>.
- Masozera, M., Bailey, M., Kerchner, C., 2007. Distribution of impacts of natural disasters across income groups: a case study of New Orleans. *Ecol. Econ.* 63 (2–3), 299–306. <https://doi.org/10.1016/j.ecolecon.2006.06.013>.
- McDaniel, C., 2017a. Irma floods tybee home: the greenville news. <https://www.greenvilleonline.com/videos/news/2017/09/13/irma-floods-tybee-home/105561810/>.
- McDaniel, C., 2017b. Tybee island emerges from irma's epic flood: the greenville news. <https://www.greenvilleonline.com/story/news/2017/09/13/tybee-island-emerges-irmas-epic-flood/659779001/>.
- Miller, D.A., White, R.A., 1998. A continuous United States multilayer soil characteristics dataset for regional climate and hydrology modeling. *Earth Interact.* 2 (2), 1–26. [https://doi.org/10.1175/1087-3562\(1998\)002<0001:ACUSMS>2.3.CO;2](https://doi.org/10.1175/1087-3562(1998)002<0001:ACUSMS>2.3.CO;2).
- Moftakhari, H.R., AghaKouchak, A., Sanders, B.F., Allaire, M., Matthew, R.A., 2018. What is nuisance flooding? Defining and monitoring an emerging challenge. *Water Resour. Res.* 54 (7), 4218–4227. <https://doi.org/10.1029/2018wr022828>.
- Moore, R.J., 1985. The probability-distributed principle and runoff production at point and basin scales. *Hydrol. Sci. J.* 30 (2), 273–297. <https://doi.org/10.1080/02626668509490989>.
- Moulds, S., Buytaert, W., Templeton, M.R., Kanu, I., 2021. Modeling the impacts of urban flood risk management on social inequality. *Water Resour. Res.* 57 (6) <https://doi.org/10.1029/2020WR029024>.
- National Academies, 2019. Framing the challenge of urban flooding in the United States. Washington, DC, USA. <https://nap.nationalacademies.org/catalog/25381/framing-the-challenge-of-urban-flooding-in-the-united-states>.
- Neal, J., Villanueva, I., Wright, N., Willis, T., Fewtrell, T., Bates, P., 2012. How much physical complexity is needed to model flood inundation? *Hydrol. Process.* 26 (15), 2264–2282. <https://doi.org/10.1002/hyp.8339>.
- Neumann, B., Vafeidis, A.T., Zimmermann, J., Nicholls, R.J., 2015. Future coastal population growth and exposure to sea-level rise and coastal flooding - a global assessment. *PLoS One* 10 (3), e0118571. <https://doi.org/10.1371/journal.pone.0118571>.
- Niazi, M., Nietch, C., Maghrebi, M., Jackson, N., Bennett, B.R., Tryby, M., Massoudieh, A., 2017. Storm water management model: performance review and gap analysis. *J. Sustain. Water Built Environ.* 3 (2). <https://doi.org/10.1061/jswbay.0000817>.
- Niu, G.-Y., Yang, Z.-L., Mitchell, K.E., Chen, F., Ek, M.B., Barlage, M., Kumar, A., Manning, K., Niyogi, D., Rosero, E., Tewari, M., Xia, Y., 2011. The community Noah land surface model with multiparameterization options (Noah-MP): 1. Model description and evaluation with local-scale measurements. *J. Geophys. Res.* 116 (D12) <https://doi.org/10.1029/2010jd015139>.
- NOAA, n.d.-a. Integrated Ocean observing systems. <https://ioos.noaa.gov/>. (Accessed 17 May 2023).
- NOAA. Tides & currents. <https://tidesandcurrents.noaa.gov/>. (Accessed 1 September 2023) n.d.-b.
- NOAA NCEI. Global historical climatology network daily (GHCNd). <https://www.ncei.noaa.gov/products/land-based-station/global-historical-climatology-network-daily>. (Accessed 1 September 2023) n.d.
- NOAA NWS. Advance hydrologic prediction service. <https://water.weather.gov/ahps/>. (Accessed 1 September 2023) n.d.
- NOAA NWS, 2016. National water model. <https://water.noaa.gov/documents/wrn-national-water-model.pdf>. (Accessed 20 November 2022).
- NOAA OCM Partners, 2012. 2009 lidar DEM: chatham, GA. <https://www.fisheries.noaa.gov/import/item/58280>. (Accessed 20 November 2022).
- Noh, S., Lee, J., Lee, S., Kawaike, K., Seo, D., 2018. Hyper-resolution 1D-2D urban flood modelling using LiDAR data and hybrid parallelization. *Environ. Model. Software* 103, 131–145. <https://doi.org/10.1016/j.envsoft.2018.02.008>.
- Noh, S., Lee, J., Lee, S., Seo, D., 2019. Retrospective dynamic inundation mapping of hurricane harvey flooding in the houston metropolitan area using high-resolution modeling and high-performance computing. *Water* 11 (3). <https://doi.org/10.3390/w11030597>.
- Ogden, F.L., 1997. CASC2D Reference Manual. Department of Civil and Environmental Engineering, University of Connecticut, p. 106.
- Ogden, F.L., Raj Pradhan, N., Downer, C.W., Zahner, J.A., 2011. Relative importance of impervious area, drainage density, width function, and subsurface storm drainage on flood runoff from an urbanized catchment. *Water Resour. Res.* 47 (12) <https://doi.org/10.1029/2011wr010550>.
- Park, K., Federico, I., Di Lorenzo, E., Ezer, T., Cobb, K.M., Pinardi, N., Coppini, G., 2022. The contribution of hurricane remote ocean forcing to storm surge along the Southeastern U.S. coast. *Coast. Eng.* 173 <https://doi.org/10.1016/j.coastaleng.2022.104098>.
- Pelling, M., Garschagen, M., 2019. Put equity first in climate adaptation. *Nature* 569 (7756), 327–329. <https://doi.org/10.1038/d41586-019-01497-9>.
- Rosenzweig, B.R., Herreros Cantis, P., Kim, Y., Cohn, A., Grove, K., Brock, J., Yesuf, J., Mistry, P., Welty, C., McPhearson, T., Sauer, J., Chang, H., 2021. The value of urban flood modeling. *Earth's Future* 9 (1). <https://doi.org/10.1029/2020ef001739>.
- Rosenzweig, C., Solecki, W., 2014. Hurricane Sandy and adaptation pathways in New York: lessons from a first-responder city. *Global Environ. Change* 28, 395–408. <https://doi.org/10.1016/j.gloenvcha.2014.05.003>.
- Rossman, L.A., 2015. Storm Water Management Model User's Manual Version 5.1. U.S. Environmental Protection Agency. https://cfpub.epa.gov/si/si_public_record_report.cfm?Lab=NRMRL&Lab=NRMRL&dirEntryId=114231.
- Rufat, S., Tate, E., Burton, C.G., Maroof, A.S., 2015. Social vulnerability to floods: review of case studies and implications for measurement. *Int. J. Disaster Risk Reduc.* 14, 470–486. <https://doi.org/10.1016/j.ijdrr.2015.09.013>.
- Saksena, S., Dey, S., Merwade, V., Singhofen, P.J., 2020. A computationally efficient and physically based approach for urban flood modeling using a flexible spatiotemporal structure. *Water Resour. Res.* 56 (1) <https://doi.org/10.1029/2019wr025769>.
- Saleh, F., Ramaswamy, V., Wang, Y., Georgas, N., Blumberg, A., Pullen, J., 2017. A multi-scale ensemble-based framework for forecasting compound coastal-riverine flooding: the Hackensack-Passaic watershed and Newark Bay. *Adv. Water Resour.* 110, 371–386. <https://doi.org/10.1016/j.advwatres.2017.10.026>.
- Salvadore, E., Bronders, J., Batelaan, O., 2015. Hydrological modelling of urbanized catchments: a review and future directions. *J. Hydrol.* 529, 62–81. <https://doi.org/10.1016/j.jhydrol.2015.06.028>.
- Santiago-Collazo, F.L., Bilsie, M.V., Hagen, S.C., 2019. A comprehensive review of compound inundation models in low-gradient coastal watersheds. *Environ. Model. Software* 119, 166–181. <https://doi.org/10.1016/j.envsoft.2019.06.002>.
- Schaake, J.C., Koren, V.I., Duan, Q.-Y., Mitchell, K., Chen, F., 1996. Simple water balance model for estimating runoff at different spatial and temporal scales. *J. Geophys. Res.* Atmos. 101 (D3), 7461–7475. <https://doi.org/10.1029/95jd02892>.
- Schmaltz, J., MODIS Land Rapid Response Team, NASA GSFC, 2017. 2017 - hurricane Irma (11L) over south Florida. https://modis.gsfc.nasa.gov/gallery/individual.php?db_date=2017-09-12. (Accessed 1 July 2023).
- Sebastian, T., Lendering, K., Kothuis, B., Brand, N., Jonkman, B., van Gelder, P., Godfroi, M., Kolen, B., Comes, T., Lhermitte, S., Meesters, K., van de Walle, B., Ebrahimi Fard, A., Cunningham, S., Khakzad, N., Nespeca, V., 2017. Hurricane harvey report: a fact-finding effort in the direct aftermath of hurricane harvey in the greater houston region. <https://resolver.tudelft.nl/uuid:54c24519-c366-4f2f-a3b9-9807db26f69c>.
- Seck, A., Welty, C., Maxwell, R.M., 2015. Spin-up behavior and effects of initial conditions for an integrated hydrologic model. *Water Resour. Res.* 51 (4), 2188–2210. <https://doi.org/10.1002/2014wr016371>.
- Shen, Y., Morsy, M.M., Huxley, C., Tahvildari, N., Goodall, J.L., 2019. Flood risk assessment and increased resilience for coastal urban watersheds under the combined impact of storm tide and heavy rainfall. *J. Hydrol.* 579 <https://doi.org/10.1016/j.jhydrol.2019.124159>.
- Shi, S., Yang, B., Jiang, W., 2022. Numerical simulations of compound flooding caused by storm surge and heavy rain with the presence of urban drainage system, coastal dam and tide gates: a case study of Xiangshan, China. *Coast. Eng.* 172 <https://doi.org/10.1016/j.coastaleng.2021.104064>.
- Silva-Araya, W., Santiago-Collazo, F.L., Gonzalez-Lopez, J., Maldonado-Maldonado, J., 2018. Dynamic modeling of surface runoff and storm surge during hurricane and tropical storm events. *Hydrology* 5 (1). <https://doi.org/10.3390/hydrology5010013>.
- Smith, M., Patrick, N., Frazier, N., Kim, J., 2021. Validation of urban flood inundation models applied using nationally available data sets: novel analyses of observed high water information. *J. Hydrol. Eng.* 26 (12) [https://doi.org/10.1061/\(asce\)he.1943-5584.0002129](https://doi.org/10.1061/(asce)he.1943-5584.0002129).
- Smart Sea Level Sensors, n.d. Smart Sea level sensors project. <https://www.sealevelsensors.org/>. (Accessed 1 September 2023).
- Smith, R.A.E., Bates, P.D., Hayes, C., 2011. Evaluation of a Coastal Flood Inundation Model Using Hard and Soft Data. *Environmental Modelling & Software*. <https://doi.org/10.1016/j.envsoft.2011.11.008>.
- Soil Conservation Service, 1972. *National Engineering Handbook, Section 4, Hydrology*. U.S. Department of Agriculture, Washington, D.C., USA.

- Soil Survey Staff, n.d. Gridded Soil Survey Geographic (gSSURGO) Database for Georgia. <https://gdg.sc.egov.usda.gov/>. (Accessed 21 November 2022).
- Sweet, W.V., Hamlington, B.D., Kopp, R.E., Weaver, C.P., Barnard, P.L., Bekaert, D., Brooks, W., Craghan, M., Dusek, G., Frederikse, T., Garner, G., Genz, A.S., Krasting, J.P., Larour, E., Marcy, D., Marra, J.J., Obeysekera, J., Osler, M., Pendleton, M., Roman, D., Schmied, L., Veatch, W., White, K.D., Zuzak, C., 2022. Global and Regional Sea Level Rise Scenarios for the United States: Updated Mean Projections and Extreme Water Level Probabilities along U.S. Coastlines. NOAA Technical Report NOS 01. National Oceanic and Atmospheric Administration. <https://oceanservice.noaa.gov/hazards/sealevelrise/noaa-nostechrpt01-global-regional-SLR-scenarios-US.pdf>.
- Sweet, W.V., Kopp, R.E., Weaver, C.P., Obeysekera, J., Horton, R.M., Thieler, E.R., Zervas, C., 2017. Global and Regional Sea Level Rise Scenarios for the United States. NOAA Technical Report NOS CO-OPS 083. National Oceanic and Atmospheric Administration. https://tidesandcurrents.noaa.gov/publications/techrpt83_Global_and_Regional_SLR_Scenarios_for_the_US_final.pdf.
- Takagi, H., Li, S., de Leon, M., Esteban, M., Mikami, T., Matsumaru, R., Shibayama, T., Nakamura, R., 2016. Storm surge and evacuation in urban areas during the peak of a storm. *Coast. Eng.* 108, 1–9. <https://doi.org/10.1016/j.coastaleng.2015.11.002>.
- Teng, J., Jakeman, A.J., Vaze, J., Croke, B.F.W., Dutta, D., Kim, S., 2017. Flood inundation modelling: a review of methods, recent advances and uncertainty analysis. *Environ. Model. Software* 90, 201–216. <https://doi.org/10.1016/j.envsoft.2017.01.006>.
- Thompson, J.R., Sørensen, H.R., Gavin, H., Refsgaard, A., 2004. Application of the coupled MIKE SHE/MIKE 11 modelling system to a lowland wet grassland in southeast England. *J. Hydrol.* 293 (1–4), 151–179. <https://doi.org/10.1016/j.jhydrol.2004.01.017>.
- USGS, n.d. Flood event viewer. <https://stn.wim.usgs.gov/FEV/>. (Accessed 1 September 2023).
- Vieux, B.E., 2001. *Distributed Hydrologic Modeling Using GIS*. Springer Science.
- Wang, Y.T., Chen, A.S., Fu, G.T., Djordjevic, S., Zhang, C., Savic, D.A., 2018. An integrated framework for high-resolution urban flood modelling considering multiple information sources and urban features. *Environ. Model. Software* 107, 85–95. <https://doi.org/10.1016/j.envsoft.2018.06.010>.
- Wickham, J., Stehman, S.V., Sorenson, D.G., Gass, L., Dewitz, J.A., 2021. Thematic accuracy assessment of the NLCD 2016 land cover for the conterminous United States. *Remote Sens. Environ.* 257 <https://doi.org/10.1016/j.rse.2021.112357>.
- Wigmosta, M.S., Lettenmaier, D.P., 1999. A comparison of simplified methods for routing topographically driven subsurface flow. *Water Resour. Res.* 35 (1), 255–264. <https://doi.org/10.1029/1998wr900017>.
- Wigmosta, M.S., Vail, L.W., Lettenmaier, D.P., 1994. A distributed hydrology-vegetation model for complex terrain. *Water Resour. Res.* 30 (6), 1665–1679. <https://doi.org/10.1029/94wr00436>.
- WTOC, 2017a. 36 hours on tybee island: before, during, and after the storm: WTOC. <https://www.wtoc.com/story/36358330/36-hours-on-tybee-island-before-during-and-after-the-storm/>.
- WTOC, 2017b. Tybee island recovery efforts continue years after hurricanes: WTOC. <https://www.wtoc.com/2019/05/30/tybee-island-recovery-efforts-continue-years-after-hurricanes/>.
- Wu, X., Wang, Z., Guo, S., Liao, W., Zeng, Z., Chen, X., 2017. Scenario-based projections of future urban inundation within a coupled hydrodynamic model framework: a case study in Dongguan City, China. *J. Hydrol.* 547, 428–442. <https://doi.org/10.1016/j.jhydrol.2017.02.020>.
- Xia, Y., Mitchell, K., Ek, M., Cosgrove, B., Sheffield, J., Luo, L., Alonge, C., Wei, H., Meng, J., Livneh, B., Duan, Q., Lohmann, D., 2012a. Continental-scale water and energy flux analysis and validation for North American Land Data Assimilation System project phase 2 (NLDAS-2): 2. Validation of model-simulated streamflow. *J. Geophys. Res. Atmos.* 117 (D3) <https://doi.org/10.1029/2011jd016051>.
- Xia, Y., Mitchell, K., Ek, M., Sheffield, J., Cosgrove, B., Wood, E., Luo, L., Alonge, C., Wei, H., Meng, J., Livneh, B., Lettenmaier, D., Koren, V., Duan, Q., Mo, K., Fan, Y., Mocko, D., 2012b. Continental-scale water and energy flux analysis and validation for the North American Land Data Assimilation System project phase 2 (NLDAS-2): 1. Intercomparison and application of model products. *J. Geophys. Res. Atmos.* 117 (D3) <https://doi.org/10.1029/2011jd016048>.
- Yang, Z.-L., Niu, G.-Y., Mitchell, K.E., Chen, F., Ek, M.B., Barlage, M., Longuevergne, L., Manning, K., Niyogi, D., Tewari, M., Xia, Y., 2011. The community Noah land surface model with multiparameterization options (Noah-MP): 2. Evaluation over global river basins. *J. Geophys. Res.* 116 (D12) <https://doi.org/10.1029/2010jd015140>.
- Yin, J., Lin, N., Yu, D., 2016. Coupled modeling of storm surge and coastal inundation: a case study in New York City during Hurricane Sandy. *Water Resour. Res.* 52 (11), 8685–8699. <https://doi.org/10.1002/2016wr019102>.
- Zhang, J., Howard, K., Langston, C., Kaney, B., Qi, Y.C., Tang, L., Grams, H., Wang, Y.D., Cocks, S., Martinaitis, S., Arthur, A., Cooper, K., Brogden, J., Kitzmiller, D., 2016. Multi-radar multi-sensor (MRMS) quantitative precipitation estimation: initial operating capabilities. *Bull. Am. Meteorol. Soc.* 97 (4), 621–637. <https://doi.org/10.1175/Bams-D-14-00174.1>.
- Zhang, J., Lin, P., Gao, S., Fang, Z., 2020. Understanding the re-infiltration process to simulating streamflow in North Central Texas using the WRF-hydro modeling system. *J. Hydrol.* 587 <https://doi.org/10.1016/j.jhydrol.2020.124902>.
- Zscheischler, J., Martius, O., Westra, S., Bevacqua, E., Raymond, C., Horton, R.M., van den Hurk, B.J.J.M., AghaKouchak, A., Jézéquel, A., Mahecha, M.D., Maraun, D., Ramos, A.M., Ridder, N.N., Thiery, W., Vignotto, E., 2020. A typology of compound weather and climate events. *Nat. Rev. Earth Environ.* 1 (7), 333–347. <https://doi.org/10.1038/s43017-020-0060-z>.